Developmental Biology 376 (2013) 74–85

Contents lists available at SciVerse ScienceDirect

Developmental Biology

journal homepage: www.elsevier.com/locate/developmentalbiology

ccm2-like is required for cardiovascular development as a novel component of the Heg-CCM pathway

Jonathan N. Rosen, Vanessa M. Sogah, Lillian Y. Ye, John D. Mably *

Boston Children's Hospital, 320 Longwood Avenue, Boston, MA 02115, United States

ARTICLE INFO

Article history:
Received 14 August 2012
Received in revised form
11 December 2012
Accepted 7 January 2013
Available online 15 January 2013

Keywords:
CCM
Cerebral cavernous malformation
ccm1
ccm2
Heg
Zebrafish

ABSTRACT

The Heart of Glass-Cerebral Cavernous Malformation (Heg-CCM) pathway is essential for normal cardiovascular development in zebrafish and mouse. In zebrafish, the Heg-CCM pathway mutants *santa (ccm1/san), valentine (ccm2/vtn)*, and *heart of glass* (heg) exhibit severely dilated hearts and inflow tracts and a complete absence of blood circulation. We identified a novel gene based on its sequence identity with *ccm2*, which we have named *ccm2-like* (*ccm2l*), and characterized its role in cardiovascular development. Disruption of *ccm2l* by morpholino injection causes dilation of the atrium and inflow tract and compromised blood circulation. Morpholino co-injection experiments identify *ccm2l* as an enhancer of the characteristic Heg-CCM dilated heart phenotype, and we find that *ccm2* overexpression can partially rescue ccm2l morphant defects. Finally, we show that Ccm2l binds Ccm1 and perform deletion and mutational analyses to define the regions of Ccm1 that mediate its binding to Ccm2l and its previously established interactors Ccm2 and Heg. These genetic and biochemical data argue that *ccm2l* is a necessary component of the Heg-CCM pathway.

Introduction

The zebrafish is tremendously useful for the identification and characterization of genes that control heart development, as both heart morphology and its functional output, blood circulation, are easily visible in the transparent, externally developing embryo. The embryonic zebrafish heart contains two chambers, one atrium and one ventricle, and each consists of two tissues: endocardium, which is a specialized endothelium that lines the inside of the heart, and the muscular myocardium that generates the contractile force. Embryos homozygous mutant for three different genes—*ccm1* (*santa/san*), *ccm2* (*valentine/vtn*), and *heart of glass* (*heg*)—exhibit the same striking phenotype: the heart and inflow tract are massively dilated, and although the heart beats, there is no blood circulation (Mably et al., 2006; Mably et al., 2003). They die around 5 days post fertilization (dpf), which is a general feature of mutants that cannot form a functional cardiovascular system. *ccm1*, *ccm2*, and *heg* are conserved across vertebrate species; their murine homologs *Ccm1*, *Ccm2*, and *Heg1*, respectively, are essential for normal cardiovascular development in mouse (Boulday et al., 2009; Kleaveland et al., 2009; Whitehead et al., 2009; Whitehead et al., 2004).

ccm1, *ccm2*, and *heg* interact genetically as components of a signaling system known as the Heart of Glass-Cerebral Cavernous Malformation (Heg-CCM) pathway. In zebrafish, slight knockdown of any of the three genes can drastically enhance heart phenotypes in embryos sensitized by a subphenotypic dose of morpholino against either of the other two (Mably et al., 2006). Similarly, the phenotype conferred by deletion of *Heg1* in mouse is enhanced in animals haploinsufficient for *Ccm2* (Kleaveland et al., 2009). CCM1, CCM2 and HEG1 proteins also interact biochemically. Co-immunoprecipitation, FRET, and yeast 2-hybrid experiments have demonstrated physical interactions between human CCM1 and CCM2 (Zawistowski et al., 2005; Zhang et al., 2007). CCM1contains three NPXY/F motifs, ankyrin repeats, and a band 4.1, ezrin, radixin, moesin (FERM) domain. CCM2 contains a phosphotyrosine binding (PTB) domain that is required for the CCM1–CCM2 interaction (Zawistowski et al., 2005). The NPXY/F motifs in CCM1 are targets of the PTB domain in CCM2, and disrupting these motifs singly or pairwise causes decreased CCM1–CCM2 binding (Zawistowski et al., 2005; Zhang et al., 2007). HEG1 is a single pass transmembrane protein whose intracellular domain binds the CCM1–CCM2 complex (Kleaveland et al., 2009).

There is strong evidence that the Heg-CCM pathway functions in the endothelium. Conditional mouse knockouts where *Ccm2* is selectively deleted from the developing endothelium phenocopy

* Correspondence to: Boston Children's Hospital, 320 Longwood Avenue, Enders 1276, Boston, MA 02115, United States.. Fax: +1 617 731 0787.
E-mail addresses: rosen.jonathan@gmail.com (J.N. Rosen), vsogah@gmail.com (V.M. Sogah), liye25@gmail.com (L.Y. Ye), john@mablylab.org (J.D. Mably).

0012-1606/$ - see front matter © 2013 Elsevier Inc. All rights reserved.
http://dx.doi.org/10.1016/j.ydbio.2013.01.006

the whole organism knockout, demonstrating that this pathway's activity is required in the endothelium (Boulday et al., 2009; Whitehead et al., 2009). *In situ* hybridization experiments in zebrafish embryos detect *heg* in the endocardium but not the myocardium, consistent with a model in which Heg-CCM signaling in the heart's endothelium regulates heart morphology (Mably et al., 2003). Adult mice heterozygous for *Ccm2* exhibit vascular leakiness (Stockton et al., 2010) and hypersensitivity to the hemorrhagic effects of VEGF injection (Whitehead et al., 2009), and this phenotype is recapitulated in endothelial cell culture where loss of *CCM1* or *CCM2* causes increased monolayer permeability (Crose et al., 2009; Glading et al., 2007; Stockton et al., 2010; Whitehead et al., 2009). These studies demonstrate that the Heg-CCM pathway is conserved across vertebrates and required in the endothelium for normal cardiovascular development and adult physiology.

The Heg-CCM pathway is so-named because mutations in the human *CCM1* and *CCM2* genes cause vascular anomalies called cerebral cavernous malformations (CCMs) (Denier et al., 2004; Laberge-le Couteulx et al., 1999; Liquori et al., 2003; Sahoo et al., 1999). CCMs, which affect approximately 0.5% of the population, are malformations of the brain vasculature characterized by an expanded endothelial vessel that can result in headache, seizure, hemorrhage and death (Revencu and Vikkula, 2006). CCMs can arise either spontaneously or as an autosomal dominant hereditary condition. In addition to *CCM1* and *CCM2*, a third gene, *CCM3*, also causes CCMs when mutated (Bergametti et al., 2005). In overexpression studies, CCM3 protein can bind CCM2 (Hilder et al., 2007; Li et al., 2010; Voss et al., 2007; Zheng et al., 2010), and knockdown of its two zebrafish homologs, *ccm3a* and *ccm3b*, affects heart development, though there are conflicting characterizations of this phenotype (Voss et al., 2009; Yoruk et al., 2012; Zheng et al., 2010). Since loss-of-function of *ccm1* and *ccm2* causes severe endothelial vessel dilation in both the embryonic zebrafish heart and the adult human brain, the zebrafish heart may provide insights into the genetic and cellular interactions that underlie human CCM disease.

Unlike other signaling pathways that have been studied extensively, the Heg-CCM pathway was discovered only recently and as a result remains incompletely understood. We employed a straightforward bioinformatic approach to identify a novel gene with sequence identity to *ccm2*, which we have named *ccm2-like* (*ccm2l*). Using morpholinos to knock down *ccm2l* in zebrafish embryos, we found that loss of *ccm2l* causes dilation of the atrium and inflow tract and a lack of blood circulation. Slight reduction of *ccm2l* causes a dilated heart phenotype in embryos sensitized by a sub-phenotypic dose of *ccm1* morpholino, defining *ccm2l* as an enhancer of the Heg-CCM pathway. Injection of *ccm2* mRNA can partially rescue cardiovascular defects in *ccm2l* morphants, suggesting that *ccm2* and *ccm2l* have overlapping *in vivo* functions. We demonstrate that Ccm2l protein binds Ccm1; moreover, we interrogate this interaction further to define the Ccm1 NPXY/F motif requirements for this interaction, which are different from those for Ccm1–Ccm2 binding. Finally, we suggest that the human homolog of *ccm2l*, *C20ORF160*, may have relevance to human CCM disease.

Materials and methods

Zebrafish

All zebrafish husbandry procedures were performed in accordance with protocols approved by the Institutional Animal Care and Use Committee at Boston Children's Hospital. Zebrafish embryos were raised in egg water at 28.5 °C. Tubingen and (*fli1*:*EGFP*)^{y1} (Lawson and Weinstein, 2002) zebrafish lines were used. For some experiments, embryos were incubated in 0.003% 1-phenyl 2-thiourea (PTU) after 1 day of development to inhibit pigment formation.

Expression analysis

In situ hybridization was performed as previously described (Mably et al., 2006; Mably et al., 2003). RT-PCR was performed either using the OneStep RT-PCR kit (Qiagen) on total RNA extracted from embryos by Trizol (Life Technologies) or by performing reverse transcription on total RNA using the QuantiTect Reverse Transcription Kit (Qiagen) followed by PCR. The following primers were used:

ccm2: 5′-CGTCTATACCGAGTCCACCA-3′, 5′- AGGAGTCTTCACTGTAGATTGAG-3′. *ccm2l*: 5′- AGGTCAAGTTCCTGGGACAC-3′, 5′- CAGACAGACTGAGAATACAGTCC-3′. *ccm1*: 5′- CATAATAGGGAAGCGTGTTGTG-3′, 5′- GGAGGAGAAATGAGCACTGG-3′. *gapdh*: 5′- GGCAAACTGGTCATTGATGG-3, 5′-CTTAATGTGAGCAGAAGCCT-3′.

cmlc2: 5′-GGAGAGAAGCTCAATGGCACA-3′, 5′-GTCATTAGCAGCCTCTTGAACTCA-3′.

insulin: 5′-GTG GAT CTC ATC TGG TCG ATG C-3′, 5′–AGG AGG AAG GAA ACC CAG AAG G-3′ (as in (Burns and MacRae, 2006)).

β-actin: 5′-GCTGTTTTCCCCTCCATTGTT-3′, 5′-TCCCATGCCAACCATCACT-3′.

Hearts were purified from whole embryos as previously described (Burns and MacRae, 2006).

Embryo microinjection

Morpholinos, designed by Gene Tools, LLC, were diluted in water to make stock solutions and further diluted in water containing a final concentration of 0.1% phenol red for injections. Embryos were injected in the yolk with 1–2 nL of diluted morpholino no later than the 2-cell stage using a PLI-100 pico-injector (Harvard Instruments) and subsequently raised at 28.5 °C. The following morpholinos were used:

ccm1: 5′-GCTTTATTTCACCTCACCTCATAGG-3′

ccm2l:MO e4i4: 5′-ACATTTCACTCTTACTAACCAGTTT-3′,

MO e2i2: 5′-TCAGACTAGACCTTGACCTCCTTCT-3′.

ccm2: 5′-GAAGCTGAGTAATACCTTAACTTCC-3′.

Standard control MO: 5′-CCTCTTACCTCAGTTACAATTTATA-3′.

In experiments to characterize the *ccm2l* knockdown phenotype, we injected 1.0 pMol MO e4i4 or 0.3 pMol MO e2i2. For enhancer experiments, pairwise combinations of morpholino were injected as single solutions. For experiments with either MO e4i4 or MO e2i2, each 1 nL injection volume contained 0.01 pMol ccm1 MO+0.05 pMol ccm2l MO, 0.01 pMol ccm1 MO+0.05 pMol standard control MO, or 0.01 pMol standard control MO+0.05 pMol ccm2l MO. The experimenter was blinded to these solutions prior to injection. For rescue experiments, embryos were first injected with morpholino (0.3 pMol MO e2i2 or 1.0 pMol MO e4i4), randomly sorted into three groups, and then injected a second time with 0.1 ng *ccm2*^{wt} mRNA or 0.1 ng *ccm2*^{m201} mRNA. (The third group was left singly injected.) The experimenter was blinded to these treatments prior to assaying phenotypes at 52 hpf.

The morpholinos against *ccm1* and *ccm2* were previously validated (Mably et al., 2006). To validate morpholinos against *ccm2l*, total RNA was isolated from embryos injected with morpholino and uninjected control embryos using Trizol reagent (Life Technologies) as per the manufacturer's instructions. The RNA was then subjected to reverse transcription PCR (RT-PCR) using the OneStep RT-PCR kit (Qiagen) with exonic primers flanking the exon-intron boundary targeted by the morpholino.

RT-PCR products were visualized by SYBR safe (Life Technologies) on an agarose gel. The following PCR primers were used:

ccm2l: 5′-TGGACTATGATCCCAAGCGAACCA-3′, 5′-GGGTTCAGGGAACAGGACACCCA-3′.

ccm2: 5′- ATGGAGGAGGATGTAAAGAA-3′, 5′- TCAGGTATCCAGGAACTGAGG -3′.

The *ccm2l* MO e2i2 and uninjected PCR products were subcloned into the PCRII-TOPO vector (Life Technologies) and sequenced.

mRNA preparation

Capped RNA was transcribed *in vitro* from linearized pCS2-ccm2, pCS2-ccm2^{m201}, and pXT7-ccm2le2i2 templates using the mMessage mMachine SP6 or T7 Ultra kits (Life Technologies) and purified using the MEGAclear kit (Life Technologies). As the last step of the purification, RNA was eluted in water and subsequently diluted in water and phenol red (final concentration of 0.1%) prior to injection.

Microscopy

Live zebrafish embryos were mounted on a microscope slide in 4% methyl cellulose without a coverslip. Imaging was accomplished on a Nikon Eclipse 90i microscope equipped with a CoolSNAP HQ2 camera (Photometrics) using NIS-Elements software. Images were subsequently processed in Adobe Photoshop.

Cloning and plasmid generation

ccm2l was cloned from cDNA reverse transcribed from total RNA isolated from 2 dpf zebrafish embryos. The following forward and reverse primers were designed with an EcoRI site and a XhoI site, respectively, to allow for subcloning of the PCR product into pCMV-HA (Clontech):

5′-GATCGAATTCAAATGGACTATGATCCCAAGCG-3′,

5′-GATCCTCGAGTCACAAGTAATAATCCTCCTC-3′.

pCMV-HA-ccm2 was generated by performing PCR on a pCS2-ccm2 template (previously described (Mably et al., 2006)) with primers containing EcoRI and XhoI restriction sites followed by digestion and ligation into pCMV-HA. The following primers were used:

5′-GATCGAATTCAAATGGAGGAGGATGTAAAGAAAG-3′,

5′-GATCCTCGAGTCAAGATGGCACGCCGTCTTG-3′.

Zebrafish *heg* was cloned into pCMV-Myc (Clontech) by performing PCR on a *heg* cDNA template (Open Biosystems clone 903796) using primers containing EcoRI and XhoI cut sites, followed by digestion and ligation. The following primers were used:

5′-GATCGAATTCAAATGATGGAAACGTGCGCTCG-3′,

5′-GATCCTCGAGTCAAAAGTAGTCTCTTCGGCGTG-3′.

Ccm1 deletion constructs were generated by performing PCR on full-length *ccm1* cDNA template with primers containing EcoRI or XhoI restriction sites and subcloning PCR fragments into pCMV-tag2b (Stratagene). The following PCR primers were used:

pCMVtag2b-ccm1:

5′-GATCGAATTCATGATGGGAAACCAAGAGCTAG-3′,

5′-GATCCTCGAGTTACCCATACGCATATTTATC-3′.

pCMVtag2b-ccm1ΔNPXY/F:

5′-GGAATTCAAATGGCAGCACAGCATGACC-3′,

5′-ACCGCTCGAGTTACCCATACGCATAT -3′.

pCMVtag2b-ccm1ΔNPXY/F-ANK:

5′-GGAATTCTGGGAGGAAACCGTGAATCTC-3′,

5′-ACCGCTCGAGTTACCCATACGCATAT -3′.

pCMVtag2b-ccm1ΔFERM:

5′-GGAATTCATGGGAAACCAAGAGCTAGAG-3′,

5′-ACCGCTCGAGGAGATTCACGGTTTCCTC-3′.

FLAG-ccm1^{ty219c} and FLAG-ccm1^{m775} were generated using the same primers and vector as pCMVtag2b-ccm1, but with PCR templates containing the appropriate *ccm1* alleles.

Point mutations were inserted in pCMVtag2b-ccm1 using the QuikChange II Site-Directed Mutagenesis Kit (Stratagene). The following primers were used:

Y193A:

5′-GTGAGTAACCCGGCGGCCGCAGTGGAGAAGCA-3,

5′-TGCTTCTCCACTGCGGCCGCCGGGTTACTCAC-3′.

Y231A:

5′-CATCCAGAACCCGCTGGCCGGCTCAGATCTGCAG-3′,

5′-CTGCAGATCTGAGCCGGCCAGCGGGTTCTGGATG-3′.

Y249A,F250A:

5′-ACAGAGTGGACAAAGTCATCATCAACCCTGCCGCTGGCTTGGGAGCTCC-3,

5′-GGAGCTCCCAAGCCAGCGGCAGGGTTGATGATGACTTTGTCCACTCTGT-3′.

pXT7-ccm2le2i2 was generated by shuttling the MO e2i2 induced RT-PCR product (*i.e.* the upper band containing an intronic insertion) from PCRII-TOPO to pXT7.

Cell culture and immunoblotting

For co-immunoprecipitation studies, 293T cells grown in Dulbecco's Modified Eagle's Media (DMEM) containing 10% fetal bovine serum were transfected at 80–100% confluence in 6-cm dishes with Lipofectamine-2000 (Life Technologies) essentially as per the manufacturer's instructions. Two days after transfection, cells were washed briefly in PBS and lysed on ice in immunoprecipitation buffer containing 30 mM Tris, 150 mM NaCl, 1% Triton X100, and Complete protease inhibitor (Roche). Lysates were agitated for ten minutes at 4 °C and then centrifuged for ten minutes at 14,000 rpm at 4 °C. Small samples of each supernatant were removed and stored at −20° to be later run on gels as inputs. The remainder of each supernatant was rocked with agarose beads conjugated to anti-FLAG antibody (Sigma) for two hours to overnight at 4 °C. Finally, beads were washed four times in cold immunoprecipitation buffer and stored at −20°.

Protein samples were diluted in NuPAGE LDS sample buffer (Life Technologies) containing DTT (final concentration 50 μM), incubated at 80 °C for ten minutes, and electrophoresed on a precast acrylamide gel (Life Technologies) at 200 V. Proteins were immobilized on PVDF paper by wet transfer at 33 V for 1–1.5 h. PVDF papers were blocked in PBS with 0.1% tween-20 (PBT) containing 5% milk and blotted with the following antibodies in blocking solution for 1 h at room temperature: FLAG M2-peroxidase 1:1000 (Sigma), HA-peroxidase 1:1000 (Roche), Heg antibody 1:500 (see next paragraph). Blots probed with anti-Heg antibody were washed three times and then incubated for one hour with peroxidase-conjugated anti-rabbit antibody (GE Healthcare) in blocking solution at 1:2500. After antibody incubation, blots were washed three times in PBT before developing with SuperSignal West Pico Substrate or SuperSignal West Dura Chemiluminescent Substrates (Thermo Scientific) as per the manufacturer's instructions.

A polyclonal antibody to the C-terminal region of Heg was generated by immunizing rabbits with a synthetic peptide designed from conceptual translation of the open reading frame. For the Heg C-terminal epitope antibody HM2148, the peptide PSFLSDDSRRRDYF was synthesized, then conjugated at the N-terminus to KLH (Keyhole Limpet Hemocyanin) through a Cys-6-carbon spacer (Princeton Biomolecules). Rabbits were injected with the peptide immunogen using a typical schedule (initial subcutaneous injection of 500 μg followed by 5 additional boosts with 250 μg at 21 day intervals; Covance Research). The terminal

exsanguination was completed at 118 days after initiation of the protocol and this serum was then affinity purified.

Results

ccm2l is a novel, conserved gene expressed during embryonic development

To identify potential homologs of genes in the Heg-CCM pathway, we queried the NCBI databases for entries with sequence identity to Heg-CCM genes using both BLASTp and BLASTx algorithms. We identified a protein bearing 43% identity to Ccm2, which we have named Ccm2-like (Ccm2l) (Fig. 1A). The coding sequence of *ccm2l* contains 1842 nucleotides and the corresponding protein has 613 amino acids. The only domain in Ccm2l readily predicted by the protein's primary sequence is a Pleckstrin-homology (PH) domain-like region comprised of amino acids 45–146 (Gough et al., 2001). The PH-like domain superfamily includes PTB domains; since the PH-like domain in Ccm2l has high identity to the PTB domain of Ccm2, we will refer to the PH-like domain as a putative PTB domain. Ccm2l and Ccm2 contain regions of high identity not only in their PTB domains, but also in their C-terminal ends (Fig. 1A,B). We amplified *ccm2l* from RNA isolated from 2-day old embryos using primers corresponding to the 5' and 3' ends of the coding region of the transcript. Sequencing of our clone revealed that it matches the full-length transcript predicted by the Ensembl Genome Browser. *ccm2l* homologs are found in other vertebrate species, including human, where it is called *C20ORF160*.

We performed RT-PCR and *in situ* hybridization to analyze when and where in the embryo *ccm2l* is expressed. By RT-PCR we found that transcripts for *ccm2l*, like *ccm1* and *ccm2*, are present at all time points we tested between fertilization and 48 h post fertilization (hpf) (Fig. 1C). The presence of transcripts at the zygote stage implies a maternal contribution of these messages. Because the Heg-CCM pathway functions in heart development, we mechanically purified 52 hpf zebrafish embryonic hearts and performed RT-PCR for *ccm1* and *ccm2l* expression, and we found that both genes are expressed in the heart (Fig. 1D). Next we performed *in situ* hybridization for *ccm2l*. We found that at 30 hpf, *ccm2l* is detectable in the presumptive notochord at the posterior

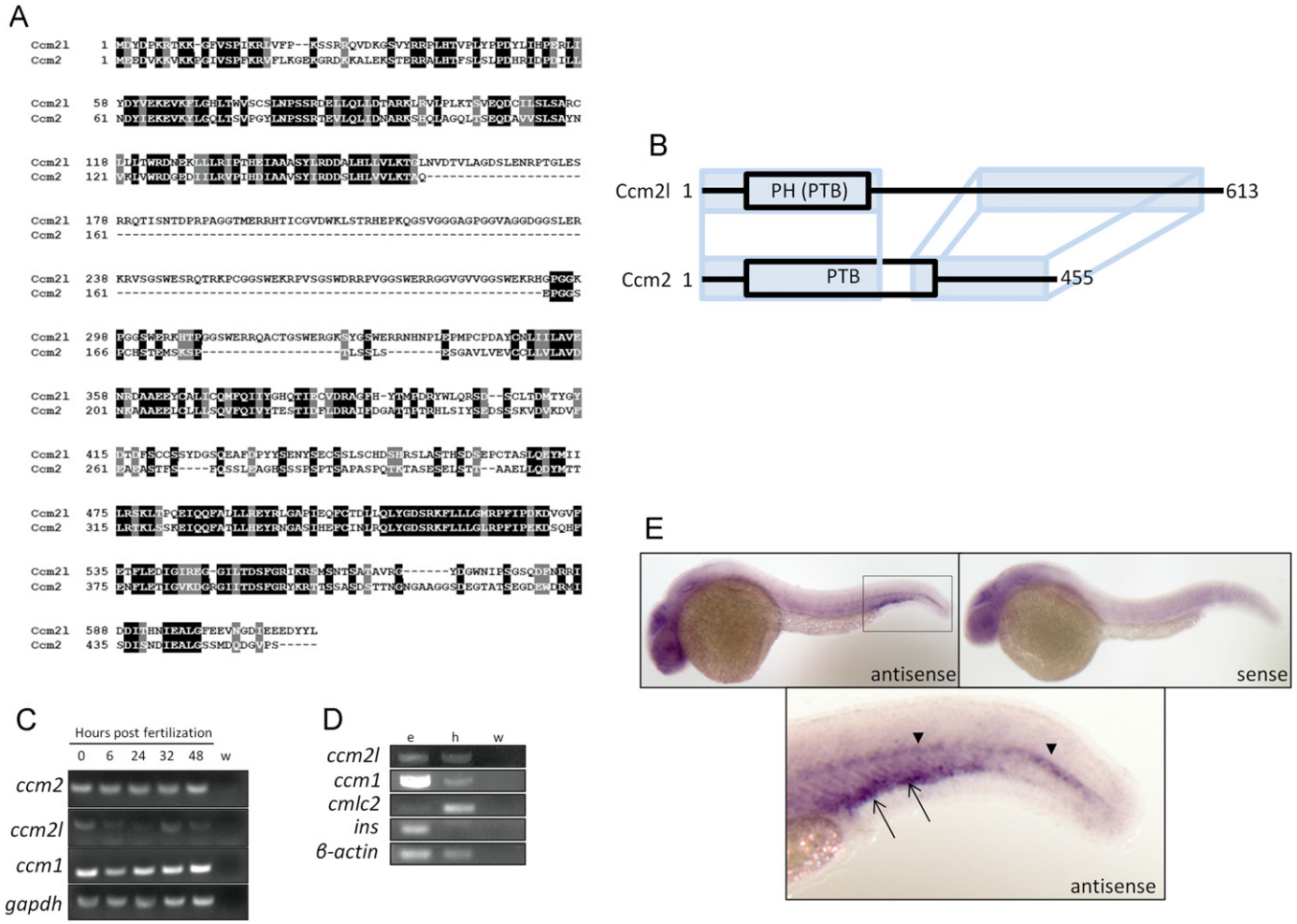

Fig. 1. Sequence and expression analysis of *ccm2l*. (A) Alignment of Ccm2l and Ccm2 protein sequences. (B) Schematic comparing the domain structures of Ccm2l and Ccm2. The N-terminal region of Ccm2l contains a putative PTB domain with high identity to the PTB domain of Ccm2. The two proteins also have regions of high identity at their C-termini. (C) RT-PCR showing expression of *ccm2*, *ccm2l*, *ccm1* and the positive control *gapdh* at five embryonic stages. All four genes are expressed at all five time points tested between 0 and 48 hpf. Water (w) is included as a negative control. (D) RT-PCR comparing expression of *ccm2l* and *ccm1* in whole embryos (e) and purified embryonic hearts (h) at 48 hpf. Both genes are expressed in the heart, with the ratio of heart expression to whole embryo expression much higher for *ccm2l*. RT-PCR for the heart-specific marker *cardiac myosin light chain* (*cmlc2*) and for a transcript absent from the heart, *insulin* (*ins*), demonstrate the quality of the heart tissue purification. (E) *In situ* hybridization analysis of *ccm2l* expression. In 30 hpf embryos, *ccm2l* expression is detected in the posterior end of the embryo in the presumptive notochord (arrowheads) and the tissue ventral to it (arrows). Embryos treated with sense probe as a negative control lack staining in these domains. PH, Pleckstrin-homology superfamily; PTB, phosphotyrosine binding domain; w, water.

end of the embryo and the tissue ventral to it; the corresponding negative control sense probe does not produce any signal in these domains (Fig. 1E). This expression pattern shares features with those of *ccm1* and *ccm2*; we have previously shown that *ccm1* is expressed in the notochord at 48 hpf and *ccm2* is expressed in the intermediate cell mass ventral to the notochord at 28 hpf (Mably et al., 2006). The mouse homolog of *ccm2l* has previously been shown to be enriched in embryonic-stem cell derived $CD31^+$ endothelial-like cells (Mariappan et al., 2009).

ccm2l is required for heart development

To characterize the role of *ccm2l* in zebrafish development, we employed a morpholino loss-of-function strategy. First, we designed a morpholino, MO e4i4, to bind an exon–intron junction in the *ccm2l* pre-mRNA. Microinjection of embryos with this morpholino caused a heart phenotype with little overall toxicity, but surprisingly, we could not detect any changes to the *ccm2l* transcript when we performed RT-PCR using primers targeted to neighboring exons. Others have reported the same phenomenon and suggested that splice site morpholinos may in some cases prevent efficient translation (Schottenfeld et al., 2007). We designed a second splice site morpholino, MO e2i2, and found that it confers a similar phenotype to MO e4i4. RT-PCR followed by sequencing demonstrated that MO e2i2 increases the amount of an endogenous alternative transcript at the expense of the expected transcript (Fig. 2A). Sequencing revealed that the alternative transcript contains an intronic inclusion with a premature stop codon (Fig. 2B); thus, MO e2i2 appears to cause a shift from normal Ccm2l protein to a severely truncated isoform. Splicing of *ccm2* at the homologous exon–intron junction is not affected (Supplemental Fig. 1).

Loss-of-function of *ccm2* in zebrafish causes a massively dilated heart phenotype (Mably et al., 2006). We began our phenotypic study of *ccm2l* by asking whether its knockdown affects heart development. At 52 hpf, uninjected embryos display compact heart chambers, a narrow inflow tract, and robust circulation (Fig. 2C,F). In contrast, we observe dilation of the atrium in 25–50% of the embryos injected with MO e2i2 (Fig. 2D,G). This heart phenotype is coincident with dilation of the inflow tract and in some embryos a complete cessation of blood circulation despite a rhythmic heart beat. At 3 dpf, we still observe dilation of the atrium (data not shown). Experiments with MO e2i2 require a relatively low dose of morpholino, as higher doses cause global developmental defects. Even at low doses, typically some embryos had to be excluded from analysis due to global defects. Embryos injected with MO e4i4 exhibit a phenotype similar to those injected with MO e2i2, consisting of dilated inflow tracts often accompanied by dilated atria at 2 dpf (Fig. 2E,H), at a lower penetrance of 18%. Heart phenotypes caused by either *ccm2l* morpholino are less severe than those observed in *ccm1*, *ccm2*, and *heg* mutants; it is unknown whether this distinction is biologically relevant or simply due to incomplete *ccm2l* knockdown.

Because our RT-PCR data show that MO e2i2 can cause heart phenotypes even though a substantial amount of normal transcript remains in the embryo, we considered the possibility that the inclusion of intron 2 generates a dominant negative protein. To test this hypothesis, we injected mRNA containing the open reading frame of this transcript and found that a small number of

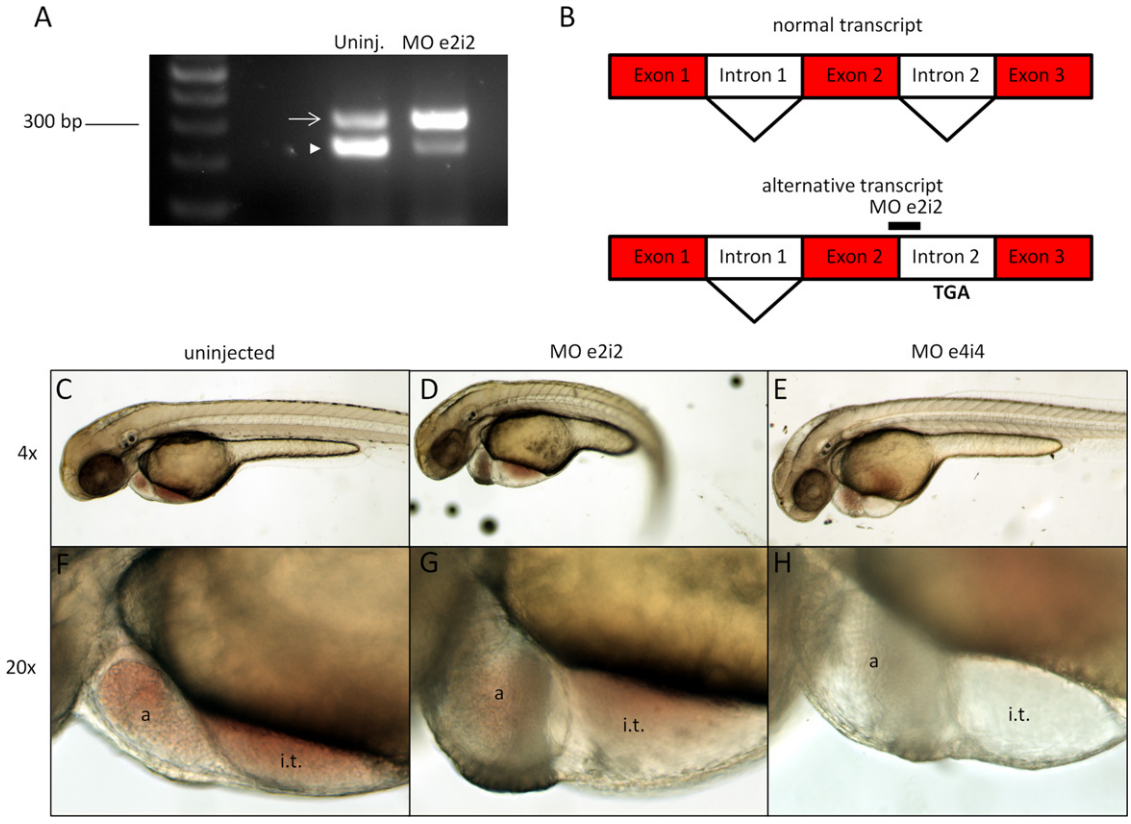

Fig. 2. *ccm2l* morphants exhibit heart and inflow tract defects. (A) Injection of MO e2i2 increases production of an endogenous alternatively spliced product (arrow) at the expense of the presumptive functional transcript (arrowhead). (B) Sequencing reveals that the alternatively spliced *ccm2l* mRNA, which is observed at increased levels in embryos injected with MO e2i2, incorporates intron 2, leading to an in-frame stop codon. (C and F) Uninjected embryos have compact heart chambers and narrow inflow tracts. (D,E,G,H) Embryos injected at the one-cell stage with 0.3 pMol MO e2i2 (D and G) or 1.0 pMol MO e4i4 (E and H) exhibit dilation of the atrium and inflow tract. Embryos injected with MO e2i2 often have a curved body axis. All images are taken from a lateral perspective with anterior to the left. a, atrium; i.t., inflow tract.

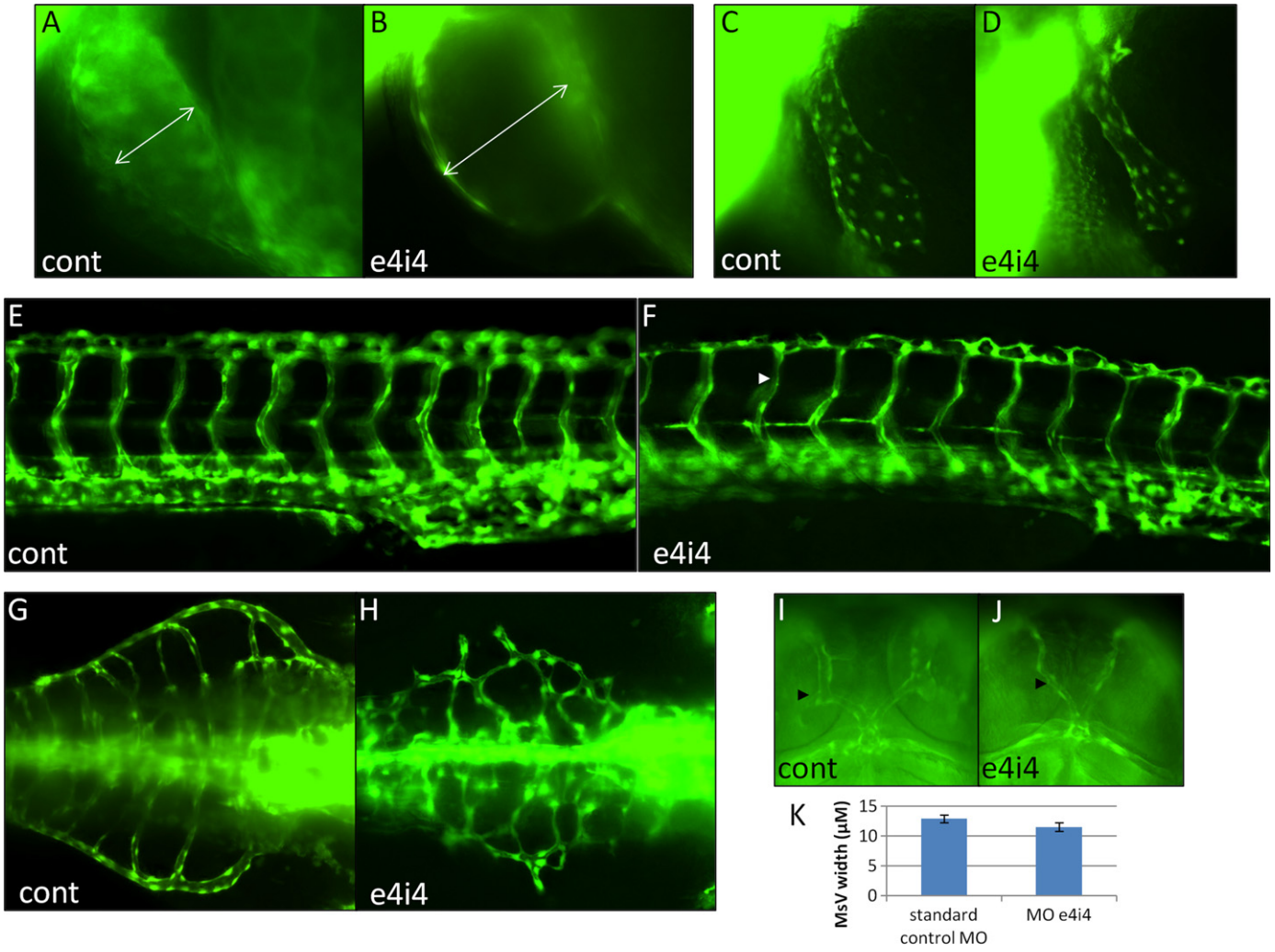

Fig. 3. Effects of *ccm2l* disruption on embryonic vasculature. (A and B) At 52 hpf, control embryos have an appropriately constricted endocardium, while *ccm2l* morphants exhibit endocardial dilation. (Arrows show lumen diameter). (C and D) Morphology of the CCV at 52 hpf is generally normal in *ccm2l* morphants. (E and F) At 58 hpf, ISVs are mostly insensitive to *ccm2l* loss-of-function, although some affected embryos have ISVs that are not fully dilated (arrowhead). (G and H) At 72 hpf, SIVs in affected embryos are frequently mispatterned. (I–K) At 52 hpf, MsVs are approximately the same width in control embryos and affected embryos (arrowheads). A and B are 20 × magnification; C–J are 10 × magnification. A–F are taken from a lateral perspective with anterior to the left; G and H are dorsal images with anterior to the right. I and J are taken from a dorsal perspective with the anterior end tilted upward. In K, error bars represent standard error. Cont, standard control morpholino.

embryos had heart or circulatory defects, but the majority appeared to have morphologically normal hearts and blood circulation (Supplemental Fig. 2 A–D). Thus, we favor the hypothesis that MO e2i2 causes a phenotype by incompletely knocking down levels of Ccm2l, not by generating a protein with dominant negative activity. Similarly, we found that morpholino against *ccm2* can confer an intermediate heart phenotype when injected at doses that allow for a substantial amount of normal transcript to endure ((Supplemental Fig. 2 E–K).

Next, we examined the effects of morpholino-mediated *ccm2l* knockdown on the embryonic vasculature using the (*fli1*:*EGFP*)^{y1} transgenic line, in which all endothelial cells are labeled with EGFP (Lawson and Weinstein, 2002). We compared the morphology of several vessels in embryos injected with a standard control morpholino (cont MO) and those injected with MO e4i4; we chose this morpholino for analysis because its low toxicity prevents secondary vascular phenotypes caused by global developmental defects. We examined the endocardium, common cardinal vein (CCV), and mesencephalic veins (MsVs) at 52 hpf, the intersegmental veins (ISVs) at 58 hpf and the subintestinal veins (SIVs) at 72 hpf. For this analysis, we selected embryos displaying heart and inflow tract defects. As expected, the morphant endocardium appears dilated compared to embryos injected with cont MO (Fig. 3A,B). The CCVs in affected embryos are generally normal (Fig. 3C,D). (We have observed some CCVs exhibiting developmental delay at 2 dpf that appear normal by 3 dpf.) We observe relatively minor defects in the ISVs and SIVs; the ISVs in affected embryos are normally patterned but a small number of vessels fail to lumenize (Fig. 3E,F), and SIVs frequently display an irregular growth pattern (Fig. 3G,H). These defects may be explained by a reduction in blood circulation, as *silent heart* (*sih*) mutants, which completely lack blood flow owing to a defect in cardiac contractility, exhibit more severe versions of those phenotypes (Hogan et al., 2008; Mably and Childs, 2010). It was recently reported that combined knockdown of *ccm3a* and *ccm3b*, but not *ccm1* or *ccm2*, causes extreme dilation of the MsVs in zebrafish, a phenotype of particular interest because of its similarity to dilated brain vessels in patients with CCM disease (Yoruk et al., 2012). We observed that MsVs in cont MO-injected embryos are approximately the same width as those in MO e4i4-injected embryos (Fig. 3I,K). Taken all together, these data suggest that *ccm2l* function may be more crucial for development of the endocardium than for the other major vessels we investigated.

ccm2l is an enhancer of the Heg-CCM pathway

The heart phenotype conferred by *ccm2l* morpholino injection is consistent with a role for *ccm2l* in the Heg-CCM pathway. To directly test whether there is a genetic interaction between *ccm2l* and the Heg-CCM pathway, we undertook a morpholino co-injection approach that we have used previously to demonstrate genetic interactions among *ccm1*, *ccm2*, and *heg* (Mably et al., 2006). We determined subphenotypic doses of *ccm2l* and *ccm1* morpholinos and injected them either together or individually with control morpholino. At 52 hpf, we assayed embryos for the dilated heart phenotype we observe in *heg*, *ccm1*, and *ccm2* mutants. Embryos were scored under light microscopy as either wildtype, intermediate, or severe. Wildtype embryos have heart morphology and blood circulation comparable to uninjected embryos; intermediate embryos have moderately dilated hearts and inflow tracks and often sluggish circulation; and severe embryos have hugely dilated hearts and inflow tracts and completely lack circulation of red blood cells (Fig. 4A). Due to the somewhat subjective nature of this rubric and the extreme sensitivity of the experiment's outcome to the precise injection volume each embryo receives, the morpholino solutions were blinded to the experimenter prior to injection and revealed after all embryos were scored.

We found that both *ccm2l* morpholinos enhance the dilated heart phenotype in embryos sensitized with *ccm1* morpholino. In experiments with MO e2i2, 49% of embryos receiving *ccm1* and *ccm2l* morpholinos had either intermediate or severe phenotypes, while only 15% of embryos that received *ccm1* morpholino with the equivalent amount of control morpholino had those phenotypes. Just 2% of embryos receiving MO e2i2 with control morpholino had a heart phenotype (Fig. 4B). In

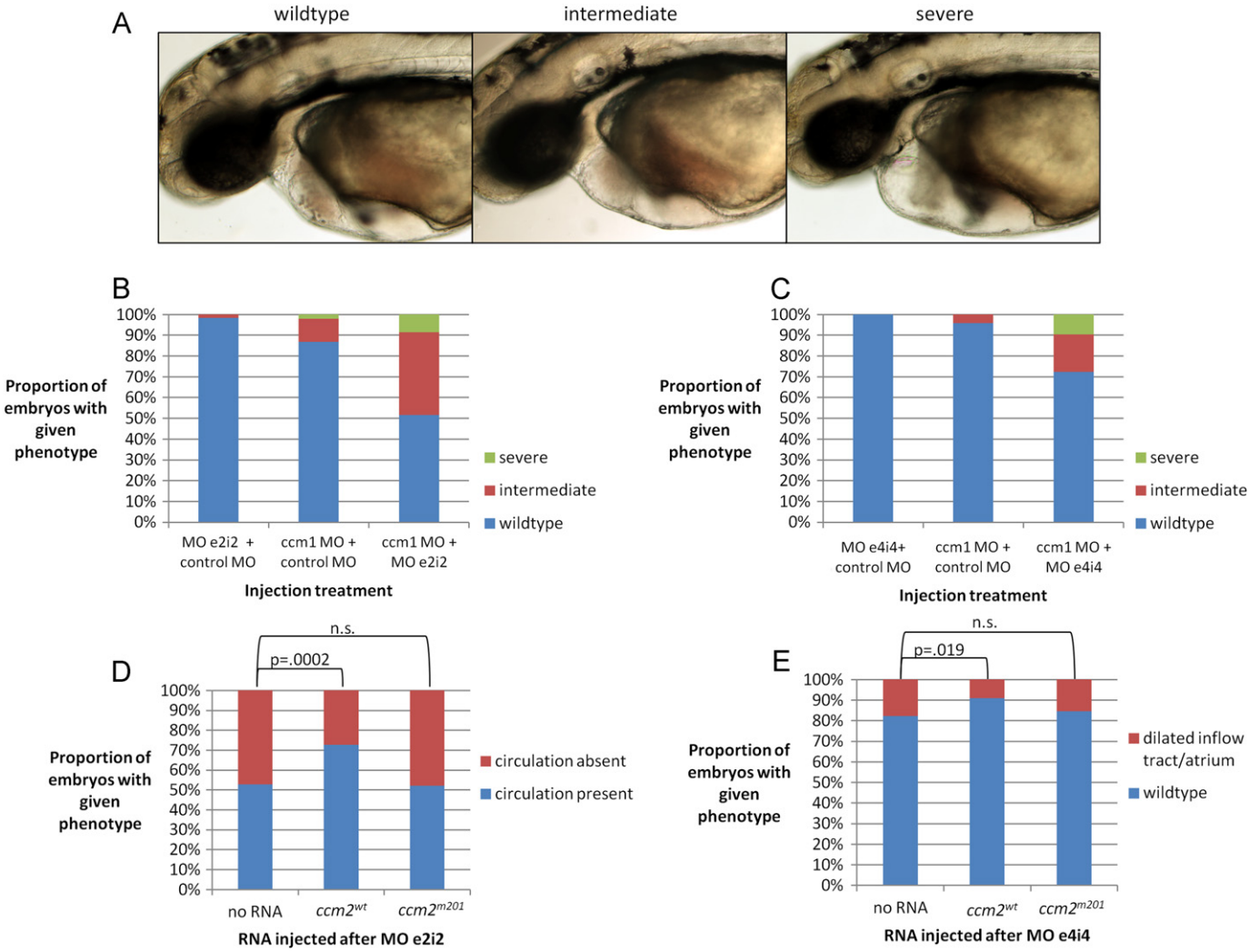

Fig. 4. *ccm2l* interacts genetically with the Heg-CCM pathway. (A–C) For enhancer experiments, embryos were injected with low doses of control morpholino, *ccm1* morpholino and *ccm2l* morpholino in pairwise combinations and assayed at 52 hpf for heart morphology and function. (A) Embryos classified as "wildtype" have a heart and inflow tract comparable to uninjected embryos and strong blood circulation. "Intermediate" embryos exhibit moderate dilation of the atrium and inflow tract but maintain some level of blood circulation. "Severe" embryos have extreme dilation of the heart and inflow tract and lack blood circulation. (B and C) Compared to a control morpholino with no predicted cellular targets, MO e2i2 and MO e4i4 both increase the proportion of moderate and severe phenotypes in embryos sensitized with *ccm1* morpholino. Images of embryos were taken at 10x magnification from a lateral perspective with anterior to the left. Graphs represent data pooled from at least three independent experiments. For each group, $n > 98$ embryos. (D,E) For rescue experiments, embryos were injected with *ccm2l* morpholino and subsequently injected with mRNA transcribed *in vitro* from either wildtype *ccm2* cDNA ($ccm2^{wt}$) or from cDNA corresponding to the *ccm2* mutant allele $ccm2^{m201}$. (D) $ccm2^{wt}$ RNA rescued circulation in a significant proportion of embryos injected with MO e2i2, while $ccm2^{m201}$ RNA did not. (E) Similarly, $ccm2^{wt}$ RNA but not $ccm2^{m201}$ RNA rescued heart and inflow tract morphology in a significant proportion of embryos injected with MO e4i4. Embryos exhibiting an enlarged inflow tract and/or enlarged atrium were labeled as "dilated inflow tract/atrium." Graphs represent data pooled from three independent experiments. For each group, $n > 130$ embryos. p-values are calculated from a 2×2 contingency table using Fisher's exact test. n.s., not significant.

experiments with MO e4i4, 28% of embryos receiving *ccm1* and *ccm2l* morpholinos had either intermediate or severe phenotypes, while only 4% of embryos that received *ccm1* morpholino with the equivalent amount of control morpholino had those phenotypes. No embryos injected with MO e4i4 and control morpholino developed abnormal heart phenotypes (Fig. 4C). We conclude that *ccm2l* is an enhancer of the Heg-CCM heart phenotype.

ccm2 overexpression partially rescues ccm2l morphant phenotypes

Due to the high degree of homology between Ccm2 and Ccm2l, our observation that their knockdown confers similar phenotypes, and our finding that *ccm2l* knockdown can enhance the heart phenotype in *ccm1* morpholino-sensitized embryos, we hypothesized that *ccm2* and *ccm2l* have overlapping *in vivo* functions. To test this hypothesis, we attempted to rescue *ccm2l* morpholino-injected embryos with synthetic *ccm2* mRNA. Since the severity of phenotype caused by our *ccm2l* morpholinos is sensitive to the volume of morpholino received by the embryo, we used a double-injection approach to insure that all groups, on average, received the same amount of *ccm2l* morpholino. First we injected a large pool of embryos with *ccm2l* morpholino and then randomly divided the pool into three groups. One group was re-injected with wildtype *ccm2* mRNA, the second group was re-injected with *ccm2* mRNA transcribed from a loss-of-function allele isolated from the zebrafish mutant *ccm2*^{m201} as a negative control, and the third group did not receive a second injection. At 52 hpf, embryos were assayed in a blind fashion.

In experiments with MO e2i2, we used circulation down the trunk of the embryo as a functional readout for cardiovascular rescue. Embryos injected with only MO e2i2 or MO e2i2 and *ccm2*^{m201} mRNA had blood circulation at rates of 53% and 52%, respectively. In contrast, embryos that received MO e2i2 and *ccm2*^{wt} mRNA had circulation at a frequency of 73% (Fig. 4D). We observed the same trend with MO e4i4. In rescue experiments with this morpholino, we scored embryos by heart and inflow tract morphology rather than blood circulation because MO e4i4 exhibits low penetrance and rarely causes circulatory block. We found that 82% and 85% of embryos injected with only MO e4i4 or MO e4i4 and *ccm2*^{m201} mRNA, respectively, had normal hearts and inflow tracts. However, 91% of embryos that received MO e4i4 and *ccm2*^{wt} mRNA had normal hearts and inflow tracts (Fig. 4E). For both morpholinos, rescue achieved by *ccm2*^{wt} mRNA was statistically significant, whereas any rescue achieved by *ccm2*^{m201} mRNA was not.

Ccm2l binds Ccm1

Next, we sought a molecular explanation for our phenotypic results linking *ccm2l* to the Heg-CCM pathway. Based on its homology to Ccm2, which is known to bind Ccm1 (Zawistowski et al., 2005; Zhang et al., 2007), we hypothesized that Ccm2l binds Ccm1 as well. To test this hypothesis, we overexpressed epitope-tagged versions of Ccm1 and Ccm2l in 293T cells, and then immunoprecipitated Ccm1 and blotted for Ccm2l. As a positive control, we performed the same experiment with Ccm1 and Ccm2. We found that both HA-ccm2 and HA-ccm2l bind

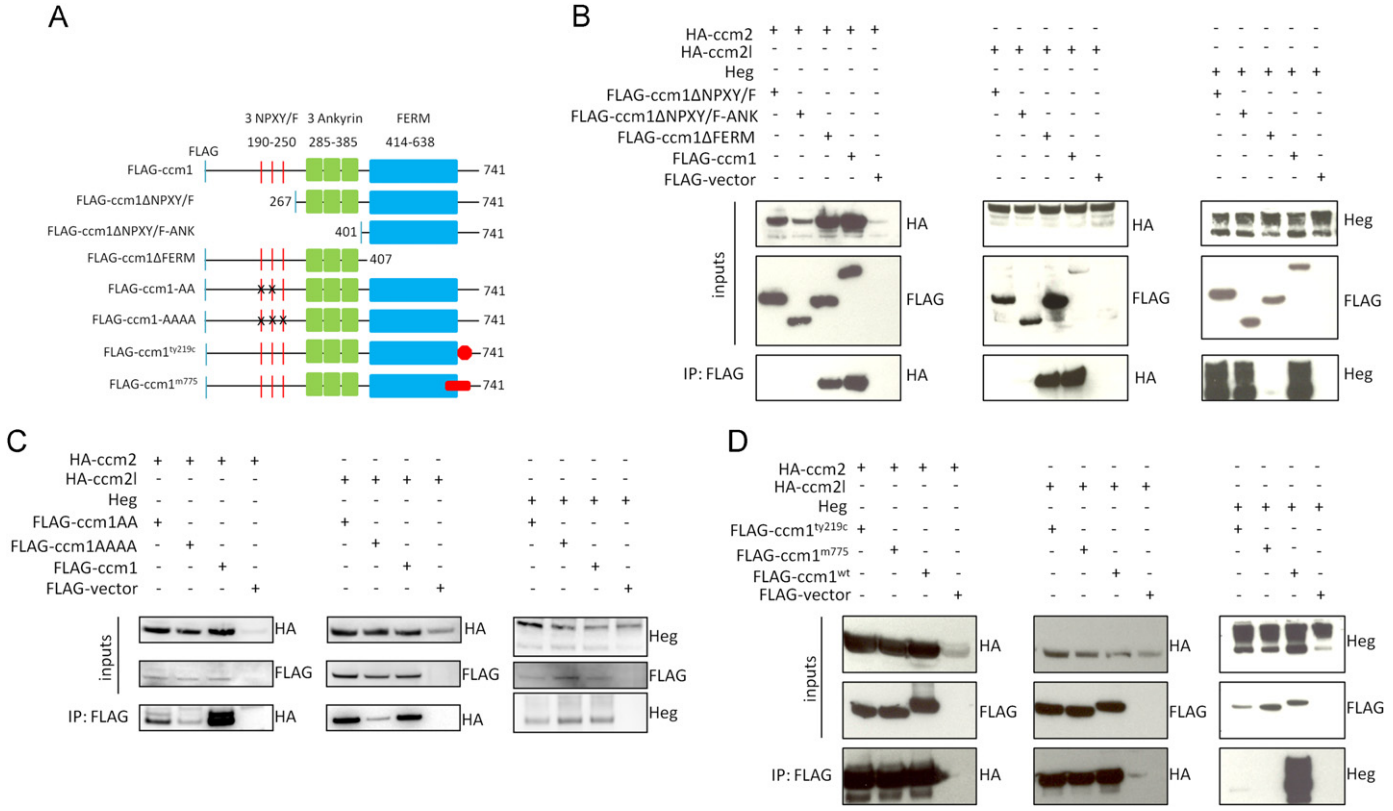

Fig. 5. Biochemical interactions among proteins of the Heg-CCM pathway. (A) Schematic of all Ccm1 constructs used for co-immunoprecipitation experiments. (B) FLAG-ccm1 and FLAG-ccm1ΔFERM co-immunoprecipitate HA-ccm2 and HA-ccm2l, while the N-terminal Ccm1 deletion proteins do not bind HA-ccm2 and HA-ccm2l. In contrast, FLAG-ccm1ΔFERM does not co-immunoprecipitate Heg, while the N-terminal Ccm1 deletion proteins do. (C) HA-ccm2 binding to FLAG-ccm1 is severely weakened by mutation of Ccm1's two NPXY motifs and further disrupted by mutations in the NPXF motif. The strength of the interaction between HA-ccm2l and FLAG-ccm1 is unaffected by mutation of Ccm1's NPXY motifs but is severely diminished when all three NPXY/F motifs are mutated. Heg-Ccm1 interactions appear unaffected by mutation of either two or all three NPXY/F motifs in Ccm1. (D) The mutant Ccm1 proteins FLAG-ccm1^{ty219c} and FLAG-ccm1^{m775} bind HA-ccm2 and HA-ccm2l as well as wildtype FLAG-ccm1 does, but they do not bind Heg.

FLAG-ccm1 (Fig. 5). Since we previously showed that *ccm1* and *ccm2l* are both expressed in the heart (Fig. 1D), this interaction in cell culture likely recapitulates an endogenous interaction.

To further define the interaction between Ccm2l and Ccm1, we performed a deletion analysis to determine which domains of Ccm1 bind Ccm2l. We generated two N-terminal Ccm1 deletion constructs, one lacking the three NPXY/F motifs and the other lacking these motifs as well as the ankyrin repeats, and a C-terminal deletion construct lacking the FERM domain. All these constructs contain an N-terminal FLAG tag (Fig. 5A). In the 293T cell overexpression system, we found that protein generated from the C-terminal deletion construct, FLAG ccm1ΔFERM, efficiently bound HA-ccm2l. In contrast, FLAG-ccm1ΔNPXY/F and FLAG-ccm1ΔNPXY/F-ANK did not bind HA-ccm2l (Fig. 5B). We observed the same result for Ccm1 binding to Ccm2 (Fig. 5B), consistent with others' work demonstrating an interaction between the N-terminal domain of human CCM1 and CCM2 (Zhang et al., 2007).

We also performed the same deletion analysis to determine which domains of Ccm1 are necessary to bind Heg, using a polyclonal antibody against Heg. We found that Ccm1 proteins with N-terminal deletions efficiently co-immunoprecipitate Heg. In contrast, Ccm1 protein lacking the FERM domain does not (Fig. 5B). We saw the same result when we replaced full-length Heg with Heg protein lacking its entire extracellular domain (Supplemental Fig. 3). Thus, the C-terminal FERM domain-containing region of Ccm1 is necessary and sufficient to bind the intracellular domain of Heg. These results are in contrast to Ccm1's interactions with Ccm2 and Ccm2l, for which the C-terminal region of Ccm1 is dispensable but the N-terminal region is essential. Consistent with our studies of the zebrafish proteins, it was recently shown that human HEG1 interacts with the FERM domain of CCM1 (Gingras et al., 2012).

The N-terminal region of zebrafish Ccm1 contains two NPXY motifs and one NPXF motif. Since Ccm2l contains a putative PTB domain, we hypothesized that the Ccm2l–Ccm1 interaction requires these motifs. To test this hypothesis, we generated two mutant *ccm1* constructs (Fig. 5A). In the first, FLAG-ccm1-AA, we altered both NPXY motifs by mutating the tyrosine residue in each to alanine. The second, FLAG-ccm1-AAAA, contains those mutations as well as two mutations in the NPXF motif. We doubly mutated the NPXF motif because the residue occupying the third position ("X") is a tyrosine. Since either the tyrosine or the phenylalanine could be mediating a protein binding interaction, we converted both to alanine. We found that FLAG-ccm1-AA binds HA-ccm2l as strongly as wildtype FLAG-ccm1, but binding of FLAG-ccm1-AAAA to HA-ccm2l is extremely diminished. In contrast, we found that the interaction between FLAG-ccm1-AA and HA-ccm2 is diminished relative to the interaction between wildtype FLAG-ccm1 and HA-ccm2, and that the interaction between FLAG-ccm1-AAAA and HA-ccm2 is weaker still (Fig. 5C). Thus, the NPXY motifs of Ccm1 are required for strong binding of Ccm1 to Ccm2 but dispensable for binding of Ccm1 to Ccm2l. As a control, we also tested the interactions between Ccm1 NPXY/F mutant proteins and Heg. Consistent with our finding that the N-terminal region of Ccm1 is not required for binding to Heg, FLAG-ccm1-AA and FLAG-ccm1-AAAA bind Heg as strongly as wildtype FLAG-Ccm1 (Fig. 5C).

Finally, we sought to determine whether the defective Ccm1 proteins produced by our *ccm1* mutant fish are capable of binding Ccm2l, Ccm2, and Heg. The mutant alleles *ccm1*^{ty219c} and *ccm1*^{m775} have a point mutation and deletion, respectively, within the 3′ end of the mRNA that are predicted to disrupt the FERM domain in both cases (Mably et al., 2006) (Fig. 5A). We subcloned these mutant alleles into expression plasmids with FLAG tags and found that both produce proteins that can bind Ccm2 and Ccm2l. However, neither mutant Ccm1 protein can bind Heg (Fig. 5D). The FERM domain of Ccm1 has been shown to bind the small GTPase RAP1 and membrane proteins such as β-CATENIN (Glading et al., 2007; Liu et al., 2011). We hypothesize that the *ccm1*^{m775} and *ccm1*^{ty219c} mutant embryos exhibit their heart phenotype owing to an inability of Ccm1 to bind these proteins as well as Heg, rather than an inability to bind Ccm2 and Ccm2l.

Discussion

ccm2l is required for normal cardiovascular development

We identified Ccm2l as a novel, conserved protein bearing considerable identity to Ccm2, and performed a loss-of-function analysis using two nonoverlapping morpholinos targeted to exon–intron junctions in the *ccm2l* pre-mRNA. *ccm2l* morphants exhibit dilation of the atrium and inflow tract and in severely affected embryos reduced or absent blood circulation. The heart and inflow tract phenotypes we observe in *ccm2l* morphants are reminiscent of but less severe than the phenotypes in *ccm1*, *ccm2*, and *heg* mutants. *ccm2l* morphants may have a more mild heart phenotype than these mutants because *ccm2l* has a more subtle role in heart development, or the difference could simply be a reflection of incomplete *ccm2l* knockdown. In the future, generation of a *ccm2l* null mutant will be crucial to resolving this ambiguity.

Morpholino disruption of *ccm2l* also confers subtle defects in other regions of the vasculature; in *ccm2l* morphants, a small number of ISVs fail to lumenize, and many SIVs have unusual growth patterns. The ISV and SIV phenotypes may be due to compromised blood flow in the embryo, since *sih* mutants, which have no blood circulation, have more severe versions of these phenotypes (Hogan et al., 2008; Mably and Childs, 2010). While we favor the interpretation that the primary function of *ccm2l* is to regulate heart morphology and the extra-cardiac vascular defects in *ccm2l* morphants are due to reduced blood circulation caused by heart dilation, we cannot yet rule out the possibility that *ccm2l* functions directly in vessels outside the heart.

Our *in situ* hybridization data showing *ccm2l* expression in the notochord and ICM do not correlate with our findings that *ccm2l* is essential for heart development. While it is possible that *ccm2l* could regulate heart morphogenesis from a distant location, we believe the more likely explanation for the discrepancy between expression pattern and phenotype is that our *in situ* hybridization protocol is insufficiently sensitive to detect *ccm2l* in the heart. In support of this reasoning, we can detect by RT-PCR *ccm2l* transcript in hearts dissociated from 2 dpf embryos. The case with *ccm1* is similar; *ccm1* is required for heart development and is detectable in purified hearts by RT-PCR, yet we have been unable to detect *ccm1* expression in the embryonic heart by *in situ* hybridization. Based on our phenotypic and RT-PCR data, as well as the literature in the field, we think that the Heg-CCM pathway, including *ccm2l*, has a tissue-autonomous function in the heart's endocardium. Tissue-specific manipulations of the Heg-CCM pathway will be required to demonstrate this.

ccm2l is a component of the Heg-CCM pathway

We conclude that *ccm2l* is a component of the Heg-CCM pathway based on four lines of evidence. First, disruption of *ccm2l* by morpholino injection causes dilation of the atrium and inflow tract. These phenotypes are less severe than those conferred by knockdown of *ccm1*, *ccm2*, or *heg,* but qualitatively similar. Second, mild knockdown of *ccm2l* enhances the dilated heart phenotype in embryos treated with a subphenotypic dose of *ccm1* morpholino. This morpholino co-injection technique was previously

used to link *heg* to the CCM pathway (Mably et al., 2006), and that finding was subsequently validated by genetic and biochemical experiments in mouse (Kleaveland et al., 2009). Third, *ccm2l* knockdown phenotypes can be partially rescued by overexpression of *ccm2*, suggesting that the two genes have partially overlapping *in vivo* functions. Fourth, Ccm2l protein can bind Ccm1.

We propose a model in which Ccm2 and Ccm2l function similarly in the Heg-CCM complex (Fig. 6). Both Ccm2 and Ccm2l bind the N-terminal region of Ccm1 through Ccm1's NPXY/F motifs, and we speculate that there is overlap between the downstream signaling events triggered by both interactions. In our model, when *ccm2l* is knocked down, exogenously supplied *ccm2* can recover the downstream signaling events that are common to the two complexes. Thus, overexpression of *ccm2* can rescue *ccm2l* morphant defects in a significant proportion of embryos. Our rescue data are also consistent with models in which *ccm2* functions downstream of *ccm2l*, but we favor the interpretation that they have interchangeable *in vivo* functions because of their structural similarity and our finding that Ccm2l, like Ccm2, binds Ccm1.

The molecular details of how Ccm2l interacts with other proteins in the Heg-CCM pathway are unknown. For example, it is unclear whether Ccm1 binds to Ccm2 and Ccm2l in a mutually exclusive manner *in vivo*, or whether Ccm2 and Ccm2l can simultaneously bind Ccm1. It is interesting to note here that the first two NPXY/F motifs in Ccm1 are jointly necessary for binding to Ccm2 but dispensable for binding to Ccm2l, which raises the possibility that Ccm2 and Ccm2l bind different NPXY/F motifs *in vivo* and might be able to bind Ccm1 simultaneously. Finer mutational analysis of the NPXY/F motifs in Ccm1 and biochemical characterization of *in vivo* Heg-CCM complexes will be required to resolve this question. Additionally, more analysis will be required to determine whether the third NPXY/F motif in Ccm1 is the site of Ccm2l binding, or whether due to redundancy, any NPXY/F motif by itself would be sufficient for binding to Ccm2l.

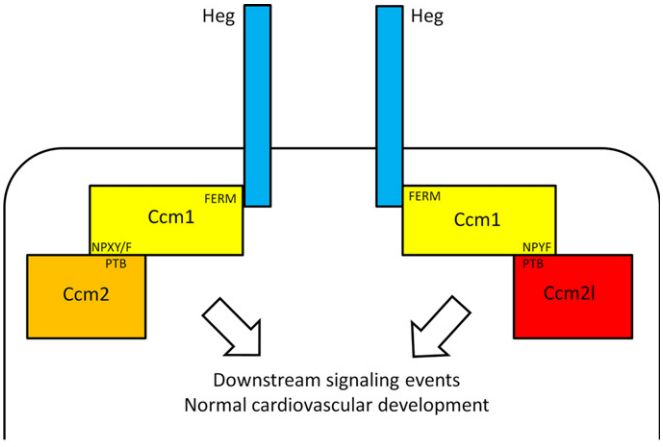

Fig. 6. Model for the function of *ccm2l* in cardiovascular development. In our model, Ccm2l binds Ccm1 through Ccm1's N-terminal region. When the two NPXY motifs in Ccm1 are disrupted, the NPYF motif is sufficient to allow binding between Ccm1 and Ccm2l. This differs from the Ccm2–Ccm1 interaction, for which the NPXY motifs are required for full-strength binding. We hypothesize that although the NPXY/F motif requirements for the Ccm1–Ccm2l and Ccm1–Ccm2 interactions differ, the two complexes transduce partially overlapping signals. Thus, when Ccm2l is reduced, exogenously supplied Ccm2 can rescue heart morphology and blood circulation in a substantial proportion of embryos. The downstream signaling events common to the Ccm1–Ccm2 and Ccm1–Ccm2l interactions are essential for normal cardiovascular development, and in their absence the endocardium and inflow tract become dilated and blood circulation is compromised.

The third NPXY/F motif, the only one of the three motifs with a phenylalanine (F) instead of a tyrosine (Y) in the fourth position, is also interesting for another reason. In general, NPXY and NPXF motifs bind similar targets but only NPXY motifs can be regulated by tyrosine phosphorylation. However, in Ccm1, the third position in the NPXF motif is occupied by a conserved tyrosine, and a recent mass spectrometry study found that this residue was the only detectable phosphotyrosine in human CCM1 (Kim et al., 2011). In future studies it will be valuable to determine whether phosphorylation at this site regulates binding of Ccm1 to Ccm2 and/or Ccm2l.

ccm2l in zebrafish and in mouse

While this paper was under review, our colleagues published a study of the function of the mouse ortholog of *ccm2l* (Zheng et al., 2012). Some of the findings of Zheng et al. on the role of *Ccm2L* in mouse are consistent with our findings on the role of *ccm2l* in zebrafish, and some are different. Zheng et al. generate a *Ccm2L* knockout mouse and find that it is viable with no gross cardiovascular defects, unlike *ccm2l* morpholino-injected zebrafish embryos that exhibit cardiac dilation. However, in a *Ccm2L*-/- background, the *Heg1*-/- phenotype is enhanced; *Heg1*-/-;*Ccm2L*+/- mice survive to birth, while *Heg1*-/-;*Ccm2L*-/- animals die in utero from cardiac defects. This elegant genetic experiment is analogous to our morpholino co-injection experiments, in which we find that slight knockdown of *ccm2l* can enhance the cardiac defects in embryos sensitized with a low dose of *ccm1* morpholino. Thus, in both zebrafish and mouse, knockdown of *Ccm2L* enhances heart defects in embryos that already have a hit to the Heg-CCM pathway. Interestingly, in mouse, this enhancement can be suppressed by loss of one allele of *Ccm2*. That is, *Heg1*-/-;*Ccm2L*-/-;*Ccm2*+/+ mice invariably die *in utero*, but a significant proportion of *Heg1*-/-;*Ccm2L*-/-;*Ccm2*+/- mice survive until birth. These genetic data arguing for antagonistic functions for *Ccm2* and *Ccm2L* contrast with our zebrafish data showing rescue of *ccm2l* knockdown phenotypes by ;overexpression of *ccm2*.

We hypothesize that the difference in the relationships between *ccm2* and *ccm2l* in zebrafish and mouse is due to the disparate mechanisms of heart growth that operate in the two species. Zheng et al. show that *Heg1*-/-;*Ccm2L*-/- hearts have a reduction in both trabeculation and expression of growth factors known to be secreted by the endocardium to promote myocardial proliferation. As a result, embryos die from inadequate heart growth, a phenotype that can be rescued by loss of one *Ccm2* allele. In zebrafish, however, neither trabeculation nor myocardial proliferation are prominent features of development during the stages of embryogenesis we examine. Trabeculation in the zebrafish ventricle does not begin until 72 hpf (Liu et al., 2010), a time point outside of the scope of our experiments. Although the number of cardiomyocytes increases between 24 and 48 hpf, proliferating cardiomyocytes are scarce; instead, the main mechanism of heart growth is the addition of newly differentiated cardiomyocytes (de Pater et al., 2009). Given the absence of trabeculation and significant myocardial proliferation, we believe the control of heart development by competitive interactions between *Ccm2* and *Ccm2L* observed by Zheng et al. in mouse would likely not be conserved in the early zebrafish embryo. It is also possible that some of the apparently species-specific differences are due to different methods of gene knockdown. In the future, it will be extremely valuable to analyze the function of *ccm2l* using a zebrafish null mutant.

The zebrafish heart as a model for CCM disease

In humans, loss-of-function mutations in *CCM1* and *CCM2* cause vascular malformations of the nervous system called CCMs. CCMs share certain features with *ccm1* and *ccm2* mutant zebrafish hearts. In both cases, vessels become severely dilated and electron microscopy reveals defects in the formation of tight junctions between endothelial cells (Kleaveland et al., 2009; Wong et al., 2000). Owing to the genetic and cell biological similarities between the dilated heart phenotype in zebrafish embryos and human CCMs, we propose that the zebrafish heart has promise as a model to understand CCM disease. In one human genetics study, only 94% and 57% of patients with familial and sporadic CCM disease, respectively, had mutations in the coding regions of the three known CCM-associated genes (Denier et al., 2006). Thus, there are likely more malformation-causing genes to be found. Moreover, CCMs range from asymptomatic to fatal, so even in patients with known disease-causing mutations there may be other genetic modifiers that influence disease severity. It stands to reason that genes that modify the *ccm1* and *ccm2* loss-of-function heart phenotypes in zebrafish may also influence CCM pathogenesis in humans. In our studies, we identify *ccm2l* as an enhancer of the dilated heart phenotype in the zebrafish embryo. We propose that the human homolog of *ccm2l*, *C20ORF160*, is an intriguing candidate gene to be investigated for mutations in patients with CCM disease of unknown genetic etiology or in patients with characterized mutations but unusually severe disease progression.

Conclusions

We conclude that *ccm2l* is essential for cardiovascular development in zebrafish due to its function in the Heg-CCM pathway. When *ccm2l* is knocked down, the embryonic atrium and inflow tract become dilated and blood flow is compromised. Slight perturbation of *ccm2l* enhances the dilated heart phenotype in embryos sensitized by morpholino against *ccm1*, defining *ccm2l* as an enhancer of the Heg-CCM pathway. Overexpression of *ccm2* partially rescues *ccm2l* morphant defects, which suggests that *ccm2* and *ccm2l* have overlapping *in vivo* functions. *ccm2l* and *ccm1* are both expressed in the heart, and Ccm2l protein binds Ccm1 in an interaction that requires Ccm1's NPXY/F motifs; however, unlike Ccm2, Ccm2l can bind Ccm1 even when the first two of the three NPXY/F motifs are mutated. Based on the role of *ccm2l* in the Heg-CCM pathway in zebrafish, the human ortholog of *ccm2l*, *C20ORF160*, may be relevant to human CCM disease.

Acknowledgments

We thank Joanne Chan and members of the Boston Children's Hospital Cardiology Division for helpful discussion, Stefanie Karwin for her care of the zebrafish, Brian Uhm and Patrick Bailey for technical assistance, and Svetlana Gapon for providing 293T cells. This work was supported by grants from the American Heart Association (11GRNT7820027 and 09PRE2261322) and the Manton Center Innovation Fund Award, Boston Children's Hospital (pilot project).

Appendix A. Supporting information

Supplementary data associated with this article can be found in the online version at http://dx.doi.org/10.1016/j.ydbio.2013.01.006.

References

Bergametti, F., Denier, C., Labauge, P., Arnoult, M., Boetto, S., Clanet, M., Coubes, P., Echenne, B., Ibrahim, R., Irthum, B., Jacquet, G., Lonjon, M., Moreau, J.J., Neau, J.P., Parker, F., Tremoulet, M., Tournier-Lasserve, E, 2005. Mutations within the programmed cell death 10 gene cause cerebral cavernous malformations. Am. J. Hum. Genet. 76, 42–51.

Boulday, G., Blecon, A., Petit, N., Chareyre, F., Garcia, L.A., Niwa-Kawakita, M., Giovannini, M., Tournier-Lasserve, E., 2009. Tissue-specific conditional CCM2 knockout mice establish the essential role of endothelial CCM2 in angiogenesis: implications for human cerebral cavernous malformations. Dis. Model Mech. 2, 168–177.

Burns, C.G., MacRae, C.A., 2006. Purification of hearts from zebrafish embryos. Biotechniques 40 274 (276), 278, passim.

Crose, L.E., Hilder, T.L., Sciaky, N., Johnson, G.L., 2009. Cerebral cavernous malformation 2 protein promotes smad ubiquitin regulatory factor 1-mediated RhoA degradation in endothelial cells. J. Biol. Chem. 284, 13301–13305.

de Pater, E., Clijsters, L., Marques, S.R., Lin, Y.F., Garavito-Aguilar, Z.V., Yelon, D., Bakkers, J., 2009. Distinct phases of cardiomyocyte differentiation regulate growth of the zebrafish heart. Development (Cambridge, England) 136, 1633–1641.

Denier, C., Goutagny, S., Labauge, P., Krivosic, V., Arnoult, M., Cousin, A., Benabid, A.L., Comoy, J., Frerebeau, P., Gilbert, B., Houtteville, J.P., Jan, M., Lapierre, F., Loiseau, H., Menei, P., Mercier, P., Moreau, J.J., Nivelon-Chevallier, A., Parker, F., Redondo, A.M., Scarabin, J.M., Tremoulet, M., Zerah, M., Maciazek, J., Tournier-Lasserve, E., 2004. Mutations within the MGC4607 gene cause cerebral cavernous malformations. Am. J. Hum. Genet. 74, 326–337.

Denier, C., Labauge, P., Bergametti, F., Marchelli, F., Riant, F., Arnoult, M., Maciazek, J., Vicaut, E., Brunereau, L., Tournier-Lasserve, E., 2006. Genotype-phenotype correlations in cerebral cavernous malformations patients. Ann. Neurol. 60, 550–556.

Gingras, A.R., Liu, J.J., Ginsberg, M.H., 2012. Structural basis of the junctional anchorage of the cerebral cavernous malformations complex. J. Cell Biol. 199, 39–48.

Glading, A., Han, J., Stockton, R.A., Ginsberg, M.H., 2007. KRIT-1/CCM1 is a Rap1 effector that regulates endothelial cell cell junctions. J. Cell Biol. 179, 247–254.

Gough, J., Karplus, K., Hughey, R., Chothia, C., 2001. Assignment of homology to genome sequences using a library of hidden Markov models that represent all proteins of known structure. J. Mol. Biol. 313, 903–919.

Hilder, T.L., Malone, M.H., Bencharit, S., Colicelli, J., Haystead, T.A., Johnson, G.L., Wu, C.C.,, 2007. Proteomic identification of the cerebral cavernous malformation signaling complex. J. Proteome Res 6, 4343–4355.

Hogan, B.M., Bussmann, J., Wolburg, H., Schulte-Merker, S., 2008. ccm1 cell autonomously regulates endothelial cellular morphogenesis and vascular tubulogenesis in zebrafish. Hum. Mol. Genet. 17, 2424–2432.

Kim, J., Sherman, N.E., Fox, J.W., Ginsberg, M.H., 2011. Phosphorylation sites in the cerebral cavernous malformations complex. J. Cell Sci. 124, 3929–3932.

Kleaveland, B., Zheng, X., Liu, J.J., Blum, Y., Tung, J.J., Zou, Z., Sweeney, S.M., Chen, M., Guo, L., Lu, M.M., Zhou, D., Kitajewski, J., Affolter, M., Ginsberg, M.H., Kahn, M.L., 2009. Regulation of cardiovascular development and integrity by the heart of glass-cerebral cavernous malformation protein pathway. Nat. Med. 15, 169–176.

Laberge-le Couteulx, S., Jung, H.H., Labauge, P., Houtteville, J.P., Lescoat, C., Cecillon, M., Marechal, E., Joutel, A., Bach, J.F., Tournier-Lasserve, E., 1999. Truncating mutations in CCM1, encoding KRIT1, cause hereditary cavernous angiomas. Nat. Genet. 23, 189–193.

Lawson, N.D., Weinstein, B.M., 2002. *In vivo* imaging of embryonic vascular development using transgenic zebrafish. Dev. Biol. 248, 307–318.

Li, X., Zhang, R., Zhang, H., He, Y., Ji, W., Min, W., Boggon, T.J., 2010. Crystal structure of CCM3, a cerebral cavernous malformation protein critical for vascular integrity. J. Biol. Chem. 285, 24099–24107.

Liquori, C.L., Berg, M.J., Siegel, A.M., Huang, E., Zawistowski, J.S., Stoffer, T., Verlaan, D., Balogun, F., Hughes, L., Leedom, T.P., Plummer, N.W., Cannella, M., Maglione, V., Squitieri, F., Johnson, E.W., Rouleau, G.A., Ptacek, L., Marchuk, D.A., 2003. Mutations in a gene encoding a novel protein containing a phosphotyrosine-binding domain cause type 2 cerebral cavernous malformations. Am. J. Hum. Genet. 73, 1459–1464.

Liu, J., Bressan, M., Hassel, D., Huisken, J., Staudt, D., Kikuchi, K., Poss, K.D., Mikawa, T., Stainier, D.Y., 2010. A dual role for ErbB2 signaling in cardiac trabeculation. Development (Cambridge, England) 137, 3867–3875.

Liu, J.J., Stockton, R.A., Gingras, A.R., Ablooglu, A.J., Han, J., Bobkov, A.A., Ginsberg, M.H., 2011. A mechanism of Rap1-induced stabilization of endothelial cell–cell junctions. Mol. Biol. Cell 22, 2509–2519.

Mably, J.D., Childs, S.J., 2010. Developmental Physiology of the Zebrafish Cardiovascular System. In: Perry, S.F., Ekker, M., Farrell, A.P., Brauner, C.J. (Eds.), Zebrafish: Fish Physiology, First ed. Academic Press, London, pp. 249–287.

Mably, J.D., Chuang, L.P., Serluca, F.C., Mohideen, M.A., Chen, J.N., Fishman, M.C., 2006. santa and valentine pattern concentric growth of cardiac myocardium in the zebrafish. Development (Cambridge, England) 133, 3139–3146.

Mably, J.D., Mohideen, M.A., Burns, C.G., Chen, J.N., Fishman, M.C., 2003. heart of glass regulates the concentric growth of the heart in zebrafish. Curr. Biol. 13, 2138–2147.

Mariappan, D., Niemann, R., Gajewski, M., Winkler, J., Chen, S., Choorapoikayil, S., Bitzer, M., Schulz, H., Hescheler, J., Sachinidis, A., 2009. Somitovasculin, a novel endothelial-specific transcript involved in the vasculature development. Arterioscler. Thromb. Vasc. Biol. 29, 1823–1829.

Revencu, N., Vikkula, M., 2006. Cerebral cavernous malformation: new molecular and clinical insights. J. Med. Genet. 43, 716–721.

Sahoo, T., Johnson, E.W., Thomas, J.W., Kuehl, P.M., Jones, T.L., Dokken, C.G., Touchman, J.W., Gallione, C.J., Lee-Lin, S.Q., Kosofsky, B., Kurth, J.H., Louis, D.N., Mettler, G., Morrison, L., Gil-Nagel, A., Rich, S.S., Zabramski, J.M., Boguski, M.S., Green, E.D., Marchuk, D.A., 1999. Mutations in the gene encoding KRIT1, a Krev-1/rap1a binding protein, cause cerebral cavernous malformations (CCM1). Hum. Mol. Genet. 8, 2325–2333.

Schottenfeld, J., Sullivan-Brown, J., Burdine, R.D., 2007. Zebrafish curly up encodes a Pkd2 ortholog that restricts left-side-specific expression of southpaw. Development (Cambridge, England) 134, 1605–1615.

Stockton, R.A., Shenkar, R., Awad, I.A., Ginsberg, M.H., 2010. Cerebral cavernous malformations proteins inhibit Rho kinase to stabilize vascular integrity. J. Exp. Med. 207, 881–896.

Voss, K., Stahl, S., Hogan, B.M., Reinders, J., Schleider, E., Schulte-Merker, S., Felbor, U., 2009. Functional analyses of human and zebrafish 18-amino acid in-frame deletion pave the way for domain mapping of the cerebral cavernous malformation 3 protein. Hum. Mutat. 30, 1003–1011.

Voss, K., Stahl, S., Schleider, E., Ullrich, S., Nickel, J., Mueller, T.D., Felbor, U., 2007. CCM3 interacts with CCM2 indicating common pathogenesis for cerebral cavernous malformations. Neurogenetics 8, 249–256.

Whitehead, K.J., Chan, A.C., Navankasattusas, S., Koh, W., London, N.R., Ling, J., Mayo, A.H., Drakos, S.G., Jones, C.A., Zhu, W., Marchuk, D.A., Davis, G.E., Li, D.Y., 2009. The cerebral cavernous malformation signaling pathway promotes vascular integrity via Rho GTPases. Nat. Med. 15, 177–184.

Whitehead, K.J., Plummer, N.W., Adams, J.A., Marchuk, D.A., Li, D.Y., 2004. Ccm1 is required for arterial morphogenesis: implications for the etiology of human cavernous malformations. Development (Cambridge, England) 131, 1437–1448.

Wong, J.H., Awad, I.A., Kim, J.H., 2000. Ultrastructural pathological features of cerebrovascular malformations: a preliminary report. Neurosurgery 46, 1454–1459.

Yoruk, B., Gillers, B.S., Chi, N.C., Scott, I.C., 2012. Ccm3 functions in a manner distinct from Ccm1 and Ccm2 in a zebrafish model of CCM vascular disease. Dev. Biol. 362, 121–131.

Zawistowski, J.S., Stalheim, L., Uhlik, M.T., Abell, A.N., Ancrile, B.B., Johnson, G.L., Marchuk, D.A., 2005. CCM1 and CCM2 protein interactions in cell signaling: implications for cerebral cavernous malformations pathogenesis. Hum. Mol. Genet. 14, 2521–2531.

Zhang, J., Rigamonti, D., Dietz, H.C., Clatterbuck, R.E., 2007. Interaction between krit1 and malcavernin: implications for the pathogenesis of cerebral cavernous malformations. Neurosurgery 60, 353–359, discussion 359.

Zheng, X., Xu, C., Di Lorenzo, A., Kleaveland, B., Zou, Z., Seiler, C., Chen, M., Cheng, L., Xiao, J., He, J., Pack, M.A., Sessa, W.C., Kahn, M.L., 2010. CCM3 signaling through sterile 20-like kinases plays an essential role during zebrafish cardiovascular development and cerebral cavernous malformations. J. Clin. Invest. 120, 2795–2804.

Zheng, X., Xu, C., Smith, A.O., Stratman, A.N., Zou, Z., Kleaveland, B., Yuan, L., Didiku, C., Sen, A., Liu, X., Skuli, N., Zaslavsky, A., Chen, M., Cheng, L., Davis, G.E., Kahn, M.L., 2012. Dynamic regulation of the cerebral cavernous malformation pathway controls vascular stability and growth. Dev. Cell 23, 342–355.